



# Microstructure and properties of laser-MIG hybrid welded joints for aluminum alloy extrusions with different gap sizes

Zhibin Yang<sup>1</sup> · Xing Wang<sup>1</sup> · Lingzhi Du<sup>1</sup>

Received: 11 July 2023 / Accepted: 30 August 2023 / Published online: 4 September 2023  
© International Institute of Welding 2023

## Abstract

Four-millimeter thick 6005A-T6/6106-T6 aluminum alloy extrusions were laser-MIG hybrid welded with different gap sizes. The influences of the gap size on the weld formation, microstructure, and mechanical properties were studied. When the gap sizes were 0 mm and 0.7 mm, the weld formation, microstructure, and mechanical properties were almost the same. The welding speed should be reduced and the arc current should be increased when the gap sizes increased to 1.0 mm and 1.5 mm, resulting in the linear energy and arc energy ratio increased. The size of the cellular dendrites increased and the grain boundaries became apparent when the gap size exceeded 1.0 mm, even cracks appeared near the fusion line when the gap size increased to 1.5 mm. The lowest microhardness existed in the heat affected zone near the fusion line when the gap size smaller than 1.0 mm, but which appeared in the weld zone when the gap size was 1.5 mm. The tensile strength slightly decreased as the gap size increased. The tensile specimens fractured near the fusion line when the gap sizes smaller than 1.0 mm and characterized by ductile fracture. The tensile specimens fractured in the heat affected zone when the gap size was 1.5 mm and characterized by ductile-brittle mixed fracture. When the gap size increased to 1.5 mm, the median fatigue limit and safe fatigue limit respectively decreased by about 26% and 30% due to the cracks existing near the fusion line in the heat affected zone.

**Keywords** Aluminum alloy extrusions · Laser-MIG hybrid welding · Microstructure · Mechanical properties · Gap size

## 1 Introduction

Aluminum alloy is one of the most common lightweight structural materials due to its low density and high strength. With the development of forming technology, the large-size aluminum alloy hollow extrusions have been widely used in the high-speed train body manufacturing industry [1, 2]. Usually, welding is the most common joining method for the aluminum alloy components. Among the various kinds of welding methods, Metal Inert Gas (MIG) welding is the most popular method because of its low cost and convenient operation, but it also has some disadvantage such as large welding deformation

and low joint strength, and which cannot meet the appearance and quality requirements of the high-speed trains [3, 4]. Laser welding has higher energy density than the conventional MIG welding, and has several outstanding advantages such as: fast welding speed, deep weld penetration, low heat input, small welding deformation, and high mechanical properties. In recent years, laser welding has gradually replaced MIG welding in some specific fields, especially in the thin plates welding. However, due to the small focusing diameter, laser welding requires extremely high assembly accuracy and has poor gap-bridging ability, which greatly limits its application and popularization [5, 6].

Laser-MIG hybrid welding couples of the laser welding and MIG welding and has the technical advantages of both, which is a promising welding method in manufacturing of aluminum alloy structural parts [7, 8]. Many studies had shown that the stable welding process and acceptable weld formation could be obtained during laser-MIG hybrid of aluminum alloys, the main reason was that the laser could stabilize the arc and the arc also could simultaneously stabilize the laser keyhole [9–11]. However, most of the

---

Recommended for publication by Commission IV - Power Beam Processes

---

✉ Zhibin Yang  
yangzhibin@djtu.edu.cn

<sup>1</sup> School of Materials Science and Engineering, Dalian Jiaotong University, 794 Huanghe Road, Shahekou District, Dalian 116028, China

researches were based on the most common butt plates welding and the gap size between the two plates was zero, which was the ideal assembly condition for the laser-MIG hybrid welding process. But the strictly zero gap size was difficult to guarantee in the actual welding practices, especially in the welding process for the length weld. Therefore, the effects of the gap size on the quality of the weld formation should be clarified, and the most important thing was to determine the allowance range of the gap size. Zhang et al. [12] showed that the gap between the plates was beneficial to improve the weld penetration due to the heat source energy could easily transmit into the deeper part of the plates. Meanwhile, several researchers indicated that some welding defects such as undercut, underfill as well as lack of fusion would be easily formed during laser-MIG hybrid welding process when the gap size was too large, and the welding efficiency decreased when the gap size increased [13–15]. According to the research results of Pellone et al. [16], a reasonable gap size could improve the appearance of the weld surface and reduce the number of the porosity defects, the main reason was that the vaporization of aluminum oxide and magnesium could be reduced when an appropriate gap size existed at the interface. Brandizzi et al. [17] demonstrated that the well-formed welds could be obtained when the gap size was no larger than 20% of the base materials thickness, and detected a slight increase in the tensile strength of the joints with increasing the gap size. Sharma et al. [18] pointed out that it had obvious benefits to enlarge the adaptability of the gap size by increasing the wire feeding speed or reducing the welding speed during the laser-MIG hybrid welding process. And the similar results were also found by Huang et al. [19] and Jing et al [20], but they also indicated that the welding process would become unstable and the weld quality would decrease when blindly increasing the wire feeding speed, the principal reason was that the droplet transfer mode changed when the gap size enlarged beyond a certain range. In conclusion, the existing researches mainly focused on the effects of gap size on the weld formation and parameter optimization for the butt plates welding. At present, the large-size aluminum alloy extrusions have been more and more widely used in

various industries, especially in the high-speed train body manufacturing industry. Therefore, it is of great significance to study the effects of the gap size on the microstructure and mechanical properties of the laser-MIG hybrid welded joints of aluminum alloy extrusions for scientific research and industrial application.

In this study, 4.0-mm thick 6005A-T6/6106-T6 aluminum alloy extrusions, which have been widely used in manufacturing of the high-speed train body, were welded by the laser-MIG hybrid welding with different gap sizes. In order to confirm the allowable range of the gap size, the influences of the gap size on the weld formation, microstructure and mechanical properties were investigated in details.

## 2 Experimental materials and methods

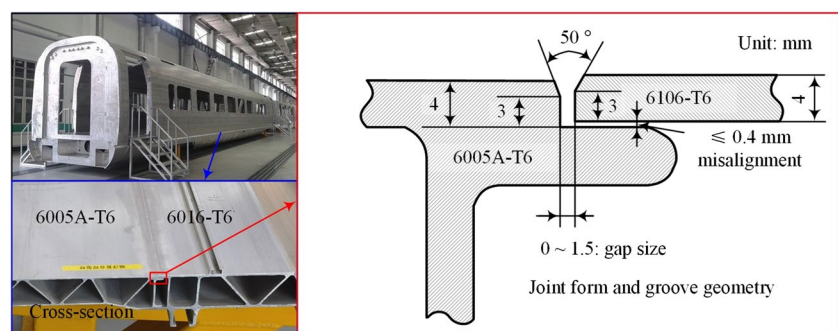
### 2.1 Materials

The base materials were 6005A-T6/6106-T6 aluminum alloy extrusions with the thickness of 4.0 mm, which have been widely used in manufacturing of the side frame structures for the high-speed train body. The size of the extrusion sample was 1000 mm × 500 mm, and its joint form and groove geometry as shown in Fig. 1. In order to remove the oxide film and greasy dirt, the surfaces of the extrusions were pretreated by mechanically grinding and wiping with acetone. The ER5356 aluminum alloy filler wire of 1.2 mm in diameter was used as the filler materials. The chemical compositions of the used materials as given in Table 1.

### 2.2 Laser-MIG hybrid welding procedure

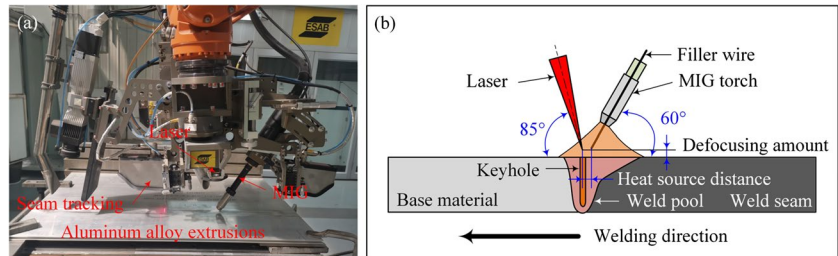
The laser-MIG hybrid welding experiments were performed by a combiner of a TRUMPF TruDisk 16003 laser and a FRONIUS TPS 5000 CMT arc welding power source, which were controlled by a KUKA KR 60 HA high-precision welding robot. The laser with the maximum power of 16 kW, and the emission wavelength was 1070 nm. The focused diameter of the laser beam could be adjusted between 0.45 and 1.6 mm. The maximum arc

**Fig. 1** Schematic diagrams of the joint form and groove geometry of the aluminum alloy extrusions



**Table 1** Chemical compositions of the used materials (wt. %)

Element	Si	Fe	Cu	Mn	Mg	Cr	Zn	Ti	Al
Base material: 6005A-T6	0.66	0.14	0.02	0.25	0.58	0.14	0.01	0.04	Bal.
Base material: 6106-T6	0.55	0.14	0.01	0.07	0.62	0.01	0.01	---	Bal.
Filler wire: ER5356	0.11	0.23	0.07	0.14	4.90	0.07	0.01	0.09	Bal.

**Fig. 2** Experimental apparatus and welding method of the laser-MIG hybrid welding: **a** experimental apparatus; **b** welding method**Table 2** Adopted laser-MIG hybrid welding parameters for different gap sizes

Parameters	Values
Gap size, $D/\text{mm}$	0, 0.3, 0.7, 1.0, 1.5
Laser power, $P/\text{kW}$	4.0, 6.0, 9.5, 9.9, 10.3
Welding speed, $V/\text{m}\cdot\text{min}^{-1}$	1.5, 2.0, 3.0
Arc current, $I/\text{A}$	180, 190, 200, 210
Defocusing amount, $h/\text{mm}$	+2, +3, +4

current of the arc welding power source was 500 A, the arc voltage and wire feeding speed could be automatically matched after the arc current preset. A laser vision seam tracking system was employed to guarantee the hybrid heat source always focused on the gap center. The experimental apparatus and welding method of the laser-MIG hybrid welding as shown in Fig. 2.

During the laser-MIG hybrid welding process, the laser was in front and the arc was in rear along the welding direction, and their inclination angles to the extrusion were  $85^\circ$  and  $60^\circ$ , respectively. The purity 99.999% of argon was used as the shielding gas, and its flow rate was 50 L/min. Based on the numerous experimental results, the heat distance was 3.0 mm and the focused diameter was 0.8 mm in this work. And the other adopted welding parameters for different gap sizes are given in Table 2. The lock butt welding structure used in this work was the fundamental reason for the gap size was not larger than 1.5 mm, the weld penetration of the bottom plate would be too deep when the gap size too large due to the laser's small spot diameter and strong penetration ability, and which was not allowed in the practical engineering applications.

## 2.3 Microstructure and property analysis

The metallographic specimens were taken from the weld cross-section, then were successively sanded, polished, etched with Keller's reagent for 15 s, and were finally observed by OLYMPUS BX-51M optical microscope. The porosity defects detected by using XXG-2505 X-ray testing instrument in the weld seam with the length of 100 mm. FM-700 microhardness tester was used to measure the microhardness distributions, the loading force was 100 g and the loading time was 10 s. The tensile properties tested by employing WDW-300 tensile testing machine, and the loading rate was  $2 \text{ mm}\cdot\text{s}^{-1}$ . The fatigue properties tested by using QBG-50 high-frequency fatigue testing machine with group method and up-down testing method, the cyclic stress ratio was 0. The surfaces of the tensile and fatigue samples were polished smooth with the weld reinforcement removed. The fracture features of the tensile and fatigue specimens were observed by using a SUPRA 55 scanning electron microscope.

## 3 Results and discussion

### 3.1 Welding parameters optimization

To meet production demands in the welding efficiency, the welding speed was fixed at  $3.0 \text{ m}\cdot\text{min}^{-1}$  when the gap size was 0 mm. Based on three factors of the laser power, arc current and defocusing amount, the orthogonal test at three different levels was used to optimize the welding parameters. The factors and levels of the orthogonal test as listed in Table 3.

The weld cross-section, surface formation and porosity defects with different welding parameters combinations of the orthogonal test when the gap size was 0 mm as shown

**Table 3** Factors and levels of the orthogonal test when the gap size was 0 mm

Levels	Factors		
	Laser power, <i>P</i> / kW A	Arc current, <i>I</i> /A B	Defocusing amount, <i>h</i> / mm C
1	9.5	190	+2
2	9.9	200	+4
3	10.3	180	+3

in Fig. 3. The results indicated that all of the welds had sufficient penetrations and moderate reinforcements, welding defects such as lack of fusion and undercut had not observed on the weld cross-sections. Meanwhile, any severe deficiency of weld surfaces like cracks, porosities and slags had not been found. The X-ray nondestructive testing results showed that there were scarcely any porosity defects existed in the weld seams. The above results indicated that the laser-MIG hybrid welding process was stable, especially the laser keyhole [21]. There were no significant differences in the weld formation quality with different welding parameters combinations. Therefore, in this work, the tensile strength was selected as the evaluation index for optimizing the welding parameters combination. The average tensile strength of the joint and its range analysis results as listed in Table 4. *K* and *R* represented the range and variance of the tensile strengths, respectively. The greater the *K* value, the greater influence of this level on the tensile strength, and the optimal level and combination of factors could be confirmed according to the *K* value. The greater the *R* value, the greater influence of this factor on the tensile strength, and the priorities of the factors could be determined according to the *R* value. Therefore, from the range analysis results, the priorities of the factors influenced on the tensile strength could be determined as follows: arc current, laser power, and defocusing amount. And the finally confirmed the optimal welding parameters combination was A2B1C2: laser power was 9.9 kW, arc current was 190 A and defocusing amount was +4 mm, which was same with the welding parameters combination of the No. 4# in Table 4.

Based on the optimal welding parameters, the adopted welding parameters for different gap sizes and the obtained weld cross-sections as shown in Fig. 4. From Fig. 4a, b, it could be found that there were no obvious welding defects observed on the weld cross-sections, the results indicated that the optimal welding parameters were also applicable to the gap sizes were 0.3 mm and 0.7 mm, except only the weld penetration slightly increased when the gap size was 0.7 mm. Therefore, in order to guarantee the weld penetration was not too deep, the laser power should be reduced as the gap size enlarged. When the gap size enlarged to 1.0

mm, with the arc current unchanged, the undercut defect appeared even if the laser power reduced to 6.0 kW and the welding speed reduced to 2.0 m·min<sup>-1</sup>, as show in Fig. 4c. The weld formation that met quality requirements could be obtained when the arc current increased to 200 A, as shown in Fig. 4d. But with the welding speed and laser power unchanged, the undercut defect still existed when the gap size enlarged to 1.5 mm even the arc current increased to 210 A, as shown in Fig. 4e, meanwhile, the weld penetration also slightly increased. With the arc current being constant, the undercut defects disappeared when the welding speed reduced to 1.5 mm, and the weld penetration was also suitable when the laser power reduced to 4.5 kW, as shown in Fig. 4f. The experimental results showed that, when the gap size enlarged, reducing welding speed was more conducive to obtaining a weld that met formation quality requirements than increasing arc current.

Figure 5 shows the results of the porosity defects detected by using X-ray testing instrument with different gap sizes using their corresponding suitable welding parameters. The results demonstrated that there were scarcely any porosity defects existing in the weld seams. Meanwhile, the results also indicated that the gap size did not have significant influences on the stabilities of the welding process and laser keyhole [22]. In conclusion, the suitable welding parameters for different gap sizes were obtained as given in Table 5. It found that the welds satisfied the quality specifications could be available using the same welding parameters when the gap size no larger than 0.7 mm, and the arc energy ratio of the total linear energy (242.3 J·mm<sup>-1</sup>) was about 26.5%. When the gap size exceeded 1.0 mm, in order to guarantee the quality of the weld formation, the welding speed and laser power should be reduced as well as the arc current should be increased, it was mostly due to the larger gap size needed more filling materials to avoid the appearance of undercut defects. Meanwhile, the results indicated that both of the linear energy and the arc energy ratio were obviously increased.

### 3.2 Microstructure features

The microstructures in the weld center of the laser-MIG hybrid welded joints with different gap sizes as shown in Fig. 6. The results indicated that the representative cellular dendrites were observed in the weld center for the four different gap sizes, only their sizes were different. When the gap sizes were 0 mm and 0.7 mm, the cellular dendrites sizes were almost the same due to using the same welding parameters, as shown in Fig. 6a, b. However, because of the increasing in the linear energy when the gap size enlarged to 1.0 mm and 1.5 mm, the cellular dendrites sizes significantly increased, as shown in Fig. 6c, d, and it would result in decrease in the microhardness of

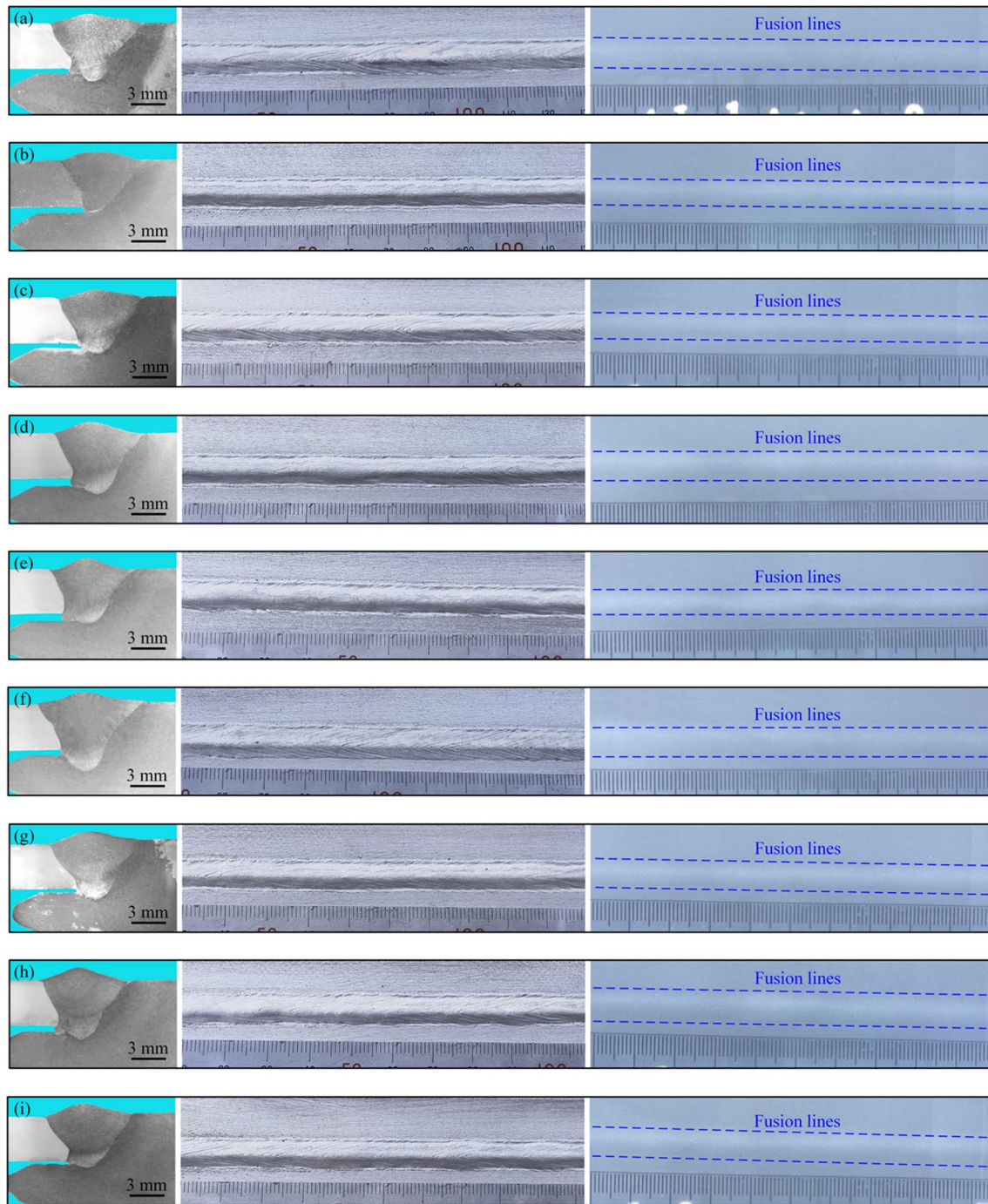


**Fig. 3** Weld cross-section, surface formation, and porosity defects with different welding parameters combinations of the orthogonal test when the gap size was 0 mm: **a**  $P = 9.5$  kW,  $I = 190$  A,  $h = +2$  mm; **b**  $P = 9.5$  kW,  $I = 200$  A,  $h = +4$  mm; **c**  $P = 9.5$  kW,  $I = 180$  A,  $h$

$= +3$  mm; **d**  $P = 9.9$  kW,  $I = 190$  A,  $h = +4$  mm; **e**  $P = 9.9$  kW,  $I = 200$  A,  $h = +3$  mm; **f**  $P = 9.9$  kW,  $I = 210$  A,  $h = +2$  mm; **g**  $P = 10.3$  kW,  $I = 190$  A,  $h = +3$  mm; **h**  $P = 10.3$  kW,  $I = 200$  A,  $h = +2$  mm; **i**  $P = 10.3$  kW,  $I = 180$  A,  $h = +4$  mm

the weld center, especially when the gap size was 1.5 mm. Figure 7 shows the microstructures in the heat affected zone of the laser-MIG hybrid welded joints with different gap sizes. The columnar zone could be observed in the weld zone closed to the fusion line, which preferentially

grew in the direction of the temperature gradient. When the gap sizes were 0 mm and 0.7 mm, the grain boundaries in columnar zone were not apparent, as shown in Fig. 7a, b. But as the gap sizes increased to 1.0 mm and 1.5 mm, the grain boundaries in the columnar zone

**Table 4** Tensile strength and its range analysis results with different welding parameters combinations when the gap size was 0 mm

No.	Laser power, $P/\text{kW}$ , A	Arc current, $I/\text{A}$ , B	Defocusing amount, $h/\text{mm}$ , C	Tensile strength $\sigma/\text{MPa}$
1#	9.5	190	+2	202.5
2#	9.5	200	+4	196.6
3#	9.5	180	+3	202.1
4#	9.9	190	+4	215.6
5#	9.9	200	+3	199.4
6#	9.9	180	+2	204.9
7#	10.3	190	+3	206.2
8#	10.3	200	+2	184.6
9#	10.3	180	+4	209.4
$K_1$	200.4	208.1	197.3	
$K_2$	206.6	193.5	207.2	
$K_3$	200.0	205.5	202.6	
$R$	6.6	14.6	9.9	
Priorities	B > C > A			
Optimization	A2	B1	C2	

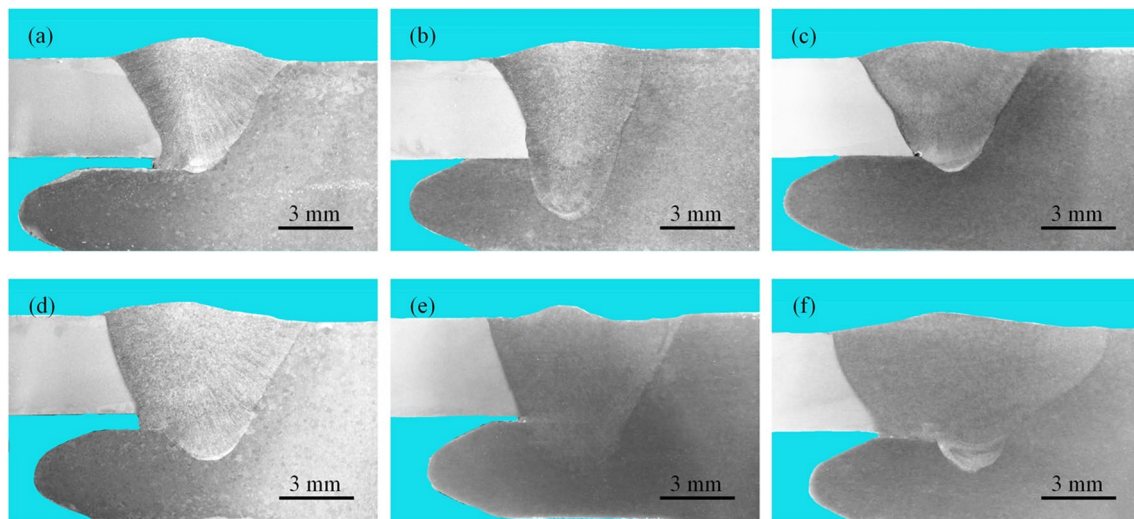


**Fig. 4** Weld cross-sections with different gap sizes and welding parameters ( $h = +4$  mm): **a**  $D = 0.3$  mm,  $V = 3.0$  m·min<sup>-1</sup>,  $P = 9.9$  kW,  $I = 190$  A; **b**  $D = 0.7$  mm,  $V = 3.0$  m·min<sup>-1</sup>,  $P = 9.9$  kW,  $I = 190$  A; **c**  $D = 1.0$  mm,  $V = 2.0$  m·min<sup>-1</sup>,  $P = 6.0$  kW,  $I = 190$  A; **d**  $D$

$= 1.0$  mm,  $V = 2.0$  m·min<sup>-1</sup>,  $P = 6.0$  kW,  $I = 200$  A; **e**  $D = 1.5$  mm,  $V = 2.0$  m·min<sup>-1</sup>,  $P = 6.0$  kW,  $I = 210$  A; **f**  $D = 1.5$  mm,  $V = 1.5$  m·min<sup>-1</sup>,  $P = 4.5$  kW,  $I = 210$  A

became apparent, and some cracks could be observed in the heat affected zone on the side of the base materials, as shown in Fig. 7c, d, the main reasons were that the higher linear energy and longer high temperature existence time [23, 24]. Therefore, it could be concluded that the microstructures deteriorated when the gap size greater than 0.7 mm, especially near the fusion line.

### 3.3 Microhardness distributions

Figure 8 provides the microhardness profiles on the weld cross-sections of the laser-MIG hybrid welded joints with different gap sizes. It could find that, for the four gap sizes, the microhardness of the weld seam and heat affected zone was lower than that of the base materials, indicating the

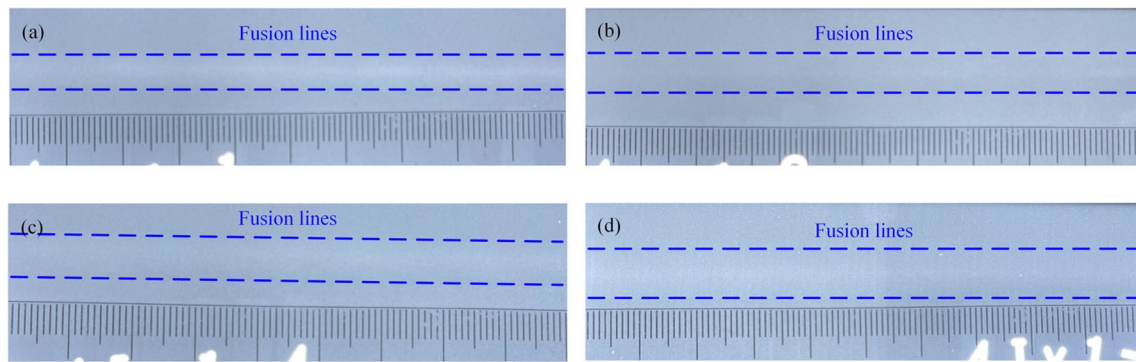


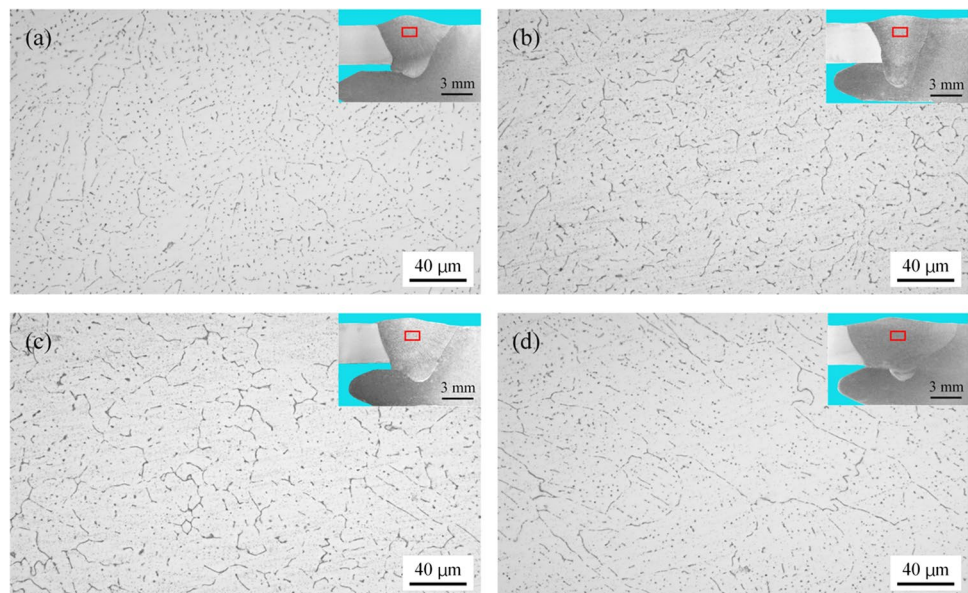
**Fig. 5** Porosity detecting results with different gap sizes using their suitable welding parameters: **a**  $D = 0.3$  mm,  $V = 3.0$  m·min<sup>-1</sup>,  $P = 9.9$  kW,  $I = 190$  A; **b**  $D = 0.7$  mm,  $V = 3.0$  m·min<sup>-1</sup>,  $P = 9.9$  kW,  $I =$

$190$  A; **c**  $D = 1.0$  mm,  $V = 2.0$  m·min<sup>-1</sup>,  $P = 6.0$  kW,  $I = 200$  A; **d**  $D = 1.5$  mm,  $V = 1.5$  m·min<sup>-1</sup>,  $P = 4.5$  kW,  $I = 210$  A

**Table 5** Adopted suitable laser-MIG hybrid welding parameters for different gap sizes

Gap size (D/mm)	Welding speed (V/m·min <sup>-1</sup> )	Laser power (P/kW)	Arc current (I/A)	Arc voltage (U/V)	Wire feeding speed (V <sub>0</sub> /m·min <sup>-1</sup> )	Linear energy (q/J·mm <sup>-1</sup> )	Arc energy ratio (φ/%)
0	3.0	9.9	190	22.5	12.2	242.3	26.5
0.3	3.0	9.9	190	22.5	12.2	242.3	26.5
0.7	3.0	9.9	190	22.5	12.2	242.3	26.5
1.0	2.0	6.0	200	22.6	12.8	263.7	38.6
1.5	1.5	4.5	210	22.8	13.4	305.6	47.0

**Fig. 6** Microstructures in the weld center of the laser-MIG hybrid welded joints with different gap sizes: **a**  $D = 0$  mm; **b**  $D = 0.7$  mm; **c**  $D = 1.0$  mm; **d**  $D = 1.5$  mm



joints had softened due to the annihilation of T6-condition caused by the heat input. The microhardness values were similar in each zone when the gap sizes were 0 mm, 0.7 mm, and 1.0 mm, and all of the lowest microhardness values were existed in the heat affected zone near the fusion line, as shown in Fig. 8a–c, the main reason for this phenomenon

was that the partial melting happened in the heat affected zone made the alloying elements in this zone more inclined to diffuse into the molten pool [25, 26]. However, when the gap size increased to 1.5 mm, the lowest microhardness value appeared in the weld zone, this change was mainly caused by the extensive burning and evaporation of the

**Fig. 7** Microstructures in the heat affected zone of the laser-MIG hybrid welded joints with different gap sizes: **a**  $D = 0$  mm; **b**  $D = 0.7$  mm; **c**  $D = 1.0$  mm; **d**  $D = 1.5$  mm

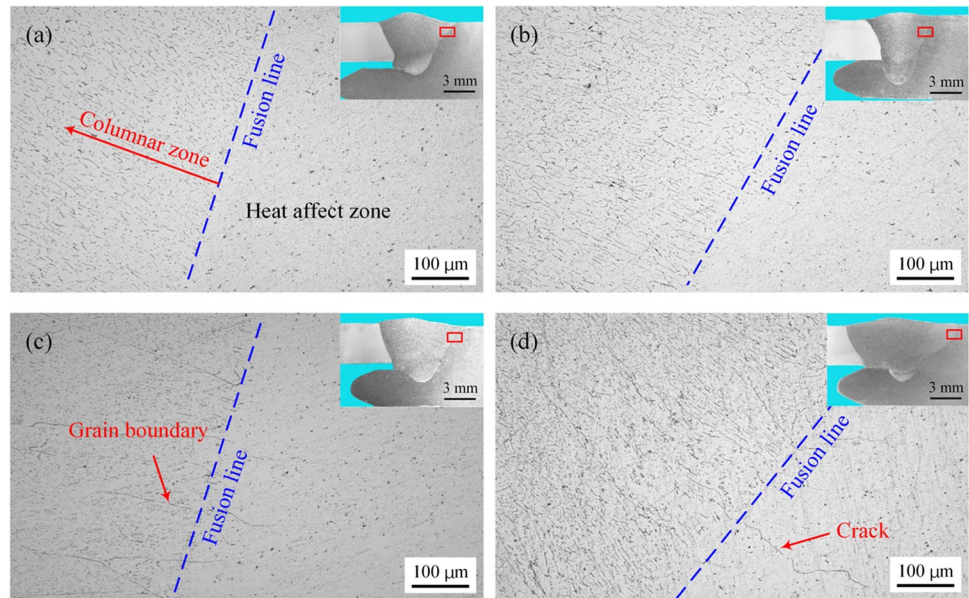
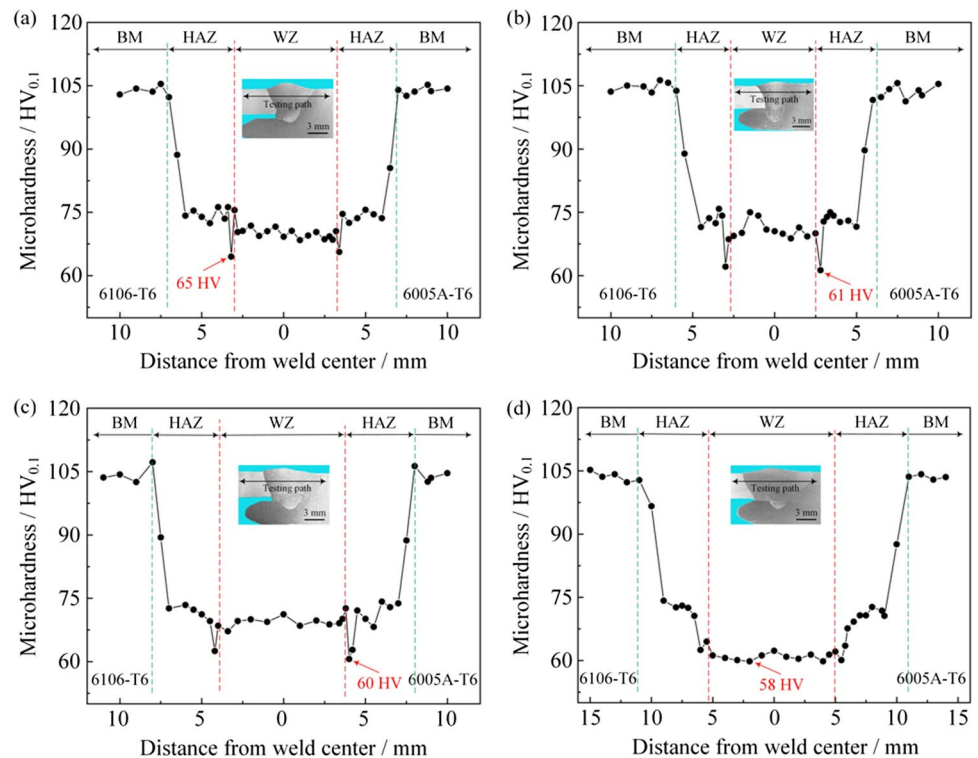


**Fig. 8** Microhardness profiles of the laser-MIG hybrid welded joints with different gap sizes: **a**  $D = 0$  mm; **b**  $D = 0.7$  mm; **c**  $D = 1.0$  mm; **d**  $D = 1.5$  mm



alloying elements in the weld molten pool due to the higher linear energy during the welding process [27]. The width of the heat affected zone was similar when the gap sizes were 0 mm and 0.7 mm, which were 3.8 mm and 3.6 mm, respectively. However, the width of the heat affected increased to 4.2 mm and 4.5 mm as the gap size increased to 1.0 mm and 1.5 mm, the increasing linear energy was the main reason and especially the increasing of the arc energy ratio.

### 3.4 Tensile properties

Table 6 lists the tensile properties of the laser-MIG hybrid welded joints with different gap sizes. The average tensile strengths were 216 MPa, 210 MPa, 210 MPa, and 208 MPa when the gap sizes were 0 mm, 0.7 mm, 1.0 mm, and 1.5 mm, which were 86.4%, 84.0%, 84.0%, and 83.2% of the base materials (250 MPa). The results indicated that the



**Table 6** Tensile testing results of the laser-MIG hybrid welded joints with different gap sizes

Gap size/mm	Average tensile strength/MPa	Joint efficiency/%	Fracture location
0	216	86.4	Near fusion line in base metal
0.7	210	84.0	Near fusion line in base metal
1.0	210	84.0	Near fusion line in base metal
1.5	208	83.2	In weld metal

tensile strength slightly reduced as the gap size increased. However, the difference was the fracture locations: all of the tensile specimens fractured near the fusion line in the base metal when the gap sizes were 0 mm, 0.7 mm, and 1.0 mm, the tensile specimens all fractured in the weld metal when the gap size was 1.5 mm. Combining with the microhardness values of each region on the weld cross-sections, it could find that the fracture locations were all located in the lowest microhardness areas. Therefore, the lowest microhardness area was the weakest area of the joints, and the reduction of the microhardness was the primary reason for the tensile strength reducing as the gap size increased.

Figure 9 shows the fracture features of the tensile specimens of the different fracture locations with different gap sizes. The fracture path was almost parallel to the fusion

line when the fracture occurred near the fusion in the base metal (gap size was 0 mm), it could be observed numerous of the distinct dimples on the fracture photograph, which indicated that the fracture mode was a typical ductile fracture, as shown in Fig. 9a, b. The fracture path and tensile specimen form an angle of approximate 45° when the fracture occurred in the weld seam (gap size was 1.5 mm), and the fracture mode was ductile-brittle mixed failure because except for the plentiful dimples there also existed some quasi-cleavage features and secondary cracks on the fracture photograph, as shown in Fig. 9c, d. Therefore, it could be concluded that the gap size had obvious effect on the fracture mode of the tensile specimen due to the change of the welding parameters.

### 3.5 Fatigue properties

Based on the comprehensive method of the group testing and up-down testing, the *S-N* fatigue curves of the laser-MIG hybrid welded joints with different gap sizes are provided in Fig. 10. The corresponding calculated median fatigue limits (survival rate was 80%), the safe fatigue limits (confidence coefficient was 95%, survival rate was 80%) and fracture locations as given in Table 7. The results indicated that the median fatigue limit and safe fatigue limit were respectively 108 MPa and 98 MPa when the gap size was 0 mm, and the specimens all fractured in the weld zone. By comparison, the fatigue properties were the same when the gap size

**Fig. 9** Fracture features of the tensile specimens of the different fracture locations with different gap sizes: **a** fracture path and **b** microscopic feature when fractured near the fusion line ( $D = 0$  mm); **c** fracture path and **d** microscopic feature when fractured in the heat affected zone ( $D = 1.5$  mm)

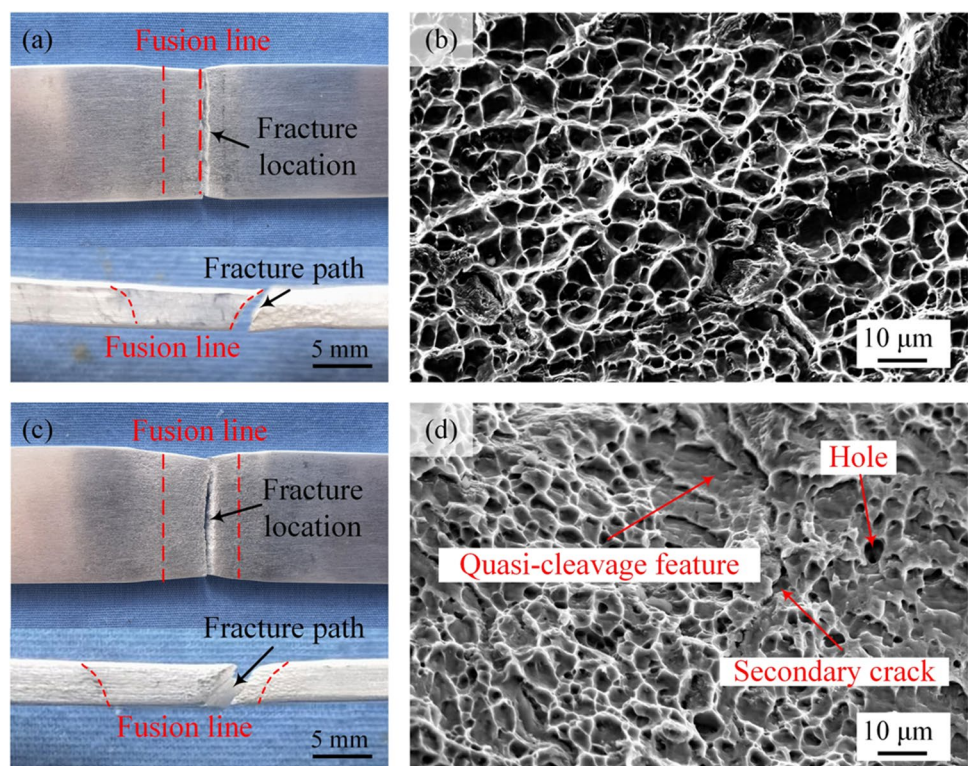


**Fig. 10** *S-N* fatigue curves of the laser-MIG hybrid welded fatigue specimens with different gap sizes: **a**  $D = 0$  mm; **b**  $D = 0.7$  mm; **c**  $D = 1.0$  mm; **d**  $D = 1.5$  mm

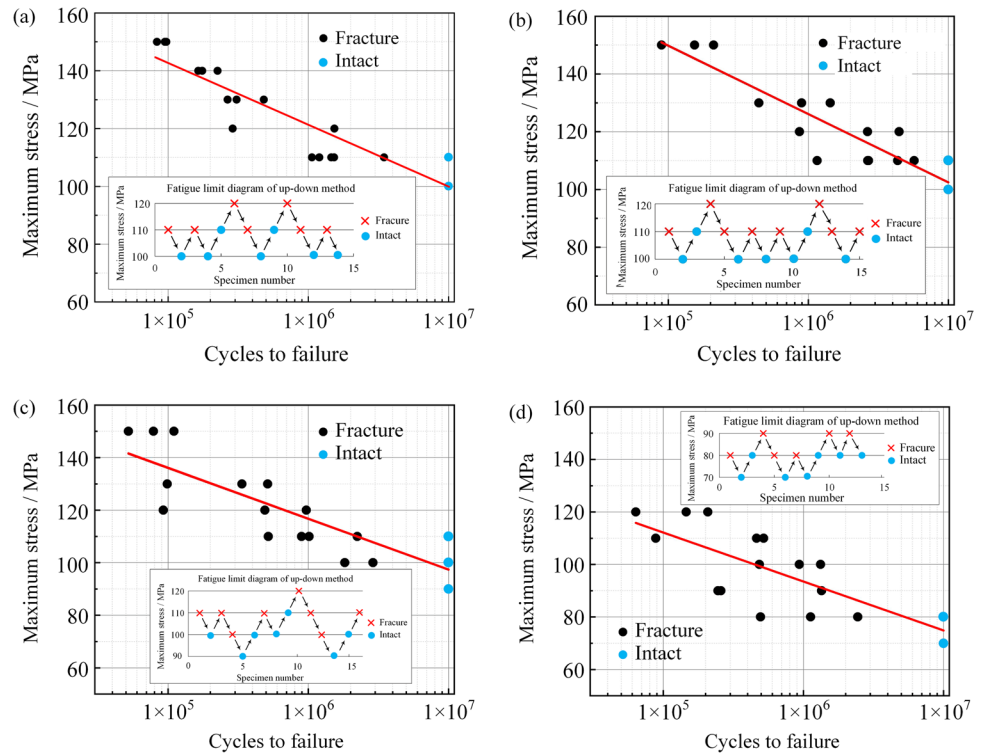


**Table 7** Fatigue testing results of the laser-MIG hybrid welded joints with different gap sizes

Gap size/mm	Median fatigue limit/MPa (survival rate was 80%)	Safe fatigue limit/MPa (confidence coefficient was 95%, survival rate was 80%)	Fracture location
0	108	98	In weld metal
0.7	108	98	In weld metal
1.0	105	93	In weld metal
1.5	80	69	Near fusion line in base metal

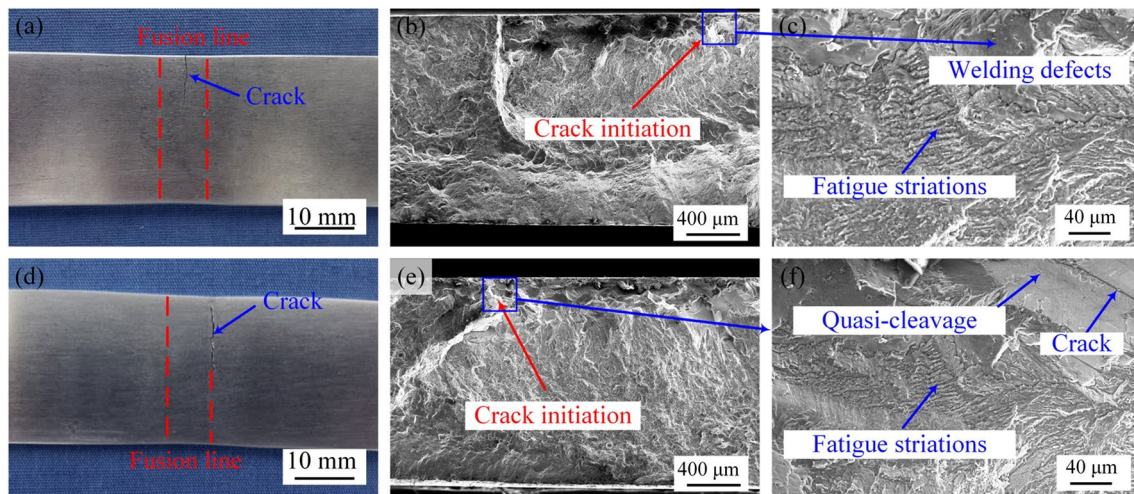
increased to 0.7 mm, and the fatigue properties slightly decreased when the gap size increased to 1.0 mm, and all of the fatigue specimens had the same fracture location: in the weld zone. However, the median fatigue limit and safe fatigue limit respectively decreased to 80 MPa and 69 MPa when the gap size increased to 1.5 mm, which respectively decreased by about 26% and 30% compared to the fatigue properties when the gap size was 0 mm, and the fracture location occurred near the fusion line in the heat affected zone instead of in the weld zone.

Figure 11 shows the fracture features of the fatigue specimens of the different fracture locations with different gap sizes. The crack initiated from minor welding defect (microstructure was not very compaction) inside the weld seam when the fracture location existed in the weld zone as shown in Fig. 11a, b, and obvious fatigue striations were found on the fracture photograph as shown in Fig. 11c. The crack initiated near the weld surface when the fracture

occurred near the fusion line in the heat affected zone close to the base metal as shown in Fig. 11d, e, besides the fatigue striations, distinct quasi-cleavage features, and cracks could also be found on the fracture photograph as shown in Fig. 11f. The cracks appeared at the grain boundaries, which would cause significant stress concentration and was the dominant reason for the greatly decreased of the fatigue properties [28], but the essential reason was still because the higher linear energy and larger arc energy ratio during the welding process when the gap size was 1.5 mm.

### 4 Conclusions

- 1) Except welding speed, the primary and secondary sequence of welding parameters affected the tensile strength was the arc current, laser power and defocusing amount. High-quality weld could be obtained by using



**Fig. 11** Fracture features of the fatigue specimens of the different fracture locations with different gap sizes: **a** fracture location, **b** macroscopic feature and **c** microscopic feature when fractured in the weld

zone ( $D = 0$  mm), **d** fracture location, **e** macroscopic feature and **f** microscopic feature when fractured near the fusion line ( $D = 1.5$  mm)

the same welding parameters when the gap sizes were 0 mm and 0.7 mm. The welding speed should be reduced and the arc current should be increased when the gap sizes increased to 1.0 mm and 1.5 mm, especially the former was more effective, meanwhile both of the linear energy and arc energy ratio increased.

- 2) The cellular dendrites existed in the weld center with different gap sizes and their sizes significantly increased when the gap sizes exceeded 1.0 mm. Meanwhile, the grain boundaries in the columnar zone became apparent when the gap sizes increased to 1.0 mm and 1.5 mm, even some cracks observed near the fusion line in the heat affected zone when the gap size increased to 1.5 mm.
- 3) The microhardness values of the weld seam and heat affected zone were lower than that of the base materials of the joints with different gap sizes due to the annihilation of T6-condition caused by the heat input. The lowest microhardness value existed in the heat affected zone near the fusion line when the gap sizes were 0 mm, 0.7 mm, and 1.0 mm, but the lowest microhardness value appeared in the weld metal when the gap size was 1.5 mm. And the width of the heat affected zone was increased when the gap sizes exceeded 1.0 mm due to the increasing linear energy and the arc energy ratio.
- 4) The average tensile strength was 216 MPa (86.4% of the base materials) when the gap size was 0 mm, and which slightly decreased as the gap size increased. The tensile specimens all fractured at the regions with the lowest microhardness value. The fracture path was almost parallel to the fusion line when the gap sizes were 0 mm, 0.7 mm, and 1.0 mm, and the fracture mode was a typical ductile fracture. The fracture occurred in the weld metal when the gap size was 1.5 mm, and the fracture mode was ductile-brittle mixed failure.

- 5) The fatigue properties were same when the gap sizes were 0 mm and 0.7 mm, the median fatigue limit and the safe fatigue limit were respectively 108 MPa and 98 MPa, which slightly decreased when the gap size increased to 1.0 mm, and fatigue specimens all fractured in the weld metal. When the gap size increased to 1.5 mm, the median fatigue limit and the safe fatigue limit respectively decreased by about 26% and 30% due to the cracks existed near the fusion line in the heat affected zone close to the base metal, which was also the reason for the fracture occurred here.

**Author contributions** All authors contributed to the study conception and design. Material preparation, data collection, and analysis were performed by Zhibin Yang, Xing Wang, and Lingzhi Du. The first draft of the manuscript was written by Zhibin Yang and all authors commented on previous versions of the manuscript. All authors read and approved the final manuscript.

**Funding** The research was supported by the Liaoning Provincial Education Department Scientific Research Foundation of China [grant number JDL2020026].

## Declarations

**Competing interests** The authors declare no competing interests.

## References

1. Lu X, Zhang C, Zhao G et al (2016) State-of-the-art of extrusion welding and proposal of a method to evaluate quantitatively welding quality during three-dimensional extrusion process. *Mater Des* 89:737–748

2. Liu X, Liu H, Wang T et al (2018) Correlation between microstructures and mechanical properties of high-speed friction stir welded aluminum hollow extrusions subjected to axial forces. *J Mater Sci Technol* 34:102–111
3. Cornacchia G, Cecchel S, Panvini A (2018) A comparative study of mechanical properties of metal inert gas (MIG)-cold metal transfer (CMT) and fiber laser-MIG hybrid welds for 6005A T6 extruded sheet. *Int J Adv Manuf Technol* 94:2017–2030
4. Du L, Yang Z, Wang X (2023) Welding characteristics of laser-MIG hybrid welding of arc-welded aluminum profiles for high-speed trains. *Materials* 16:404
5. Volpp J (2022) Multispot laser welding for increased gap bridgability. *J Laser Appl* 34:042002
6. Schultz V, Seefeld T, Vollertsen F (2014) Gap bridging ability in laser beam welding of thin aluminum sheets. *Phys Procedia* 56:545–553
7. Acherjee B (2018) Hybrid laser arc welding: state-of-art review. *Opt Laser Technol* 99:60–71
8. Chen C, Shen Y, Gao M et al (2020) Influence of welding angle on the weld morphology and porosity in laser-arc hybrid welding of AA2219 aluminum alloy. *Weld World* 64:37–45
9. Hu B, Den Ouden G (2005) Laser induced stabilisation of the welding arc. *Sci Technol Weld Join* 10:76–81
10. Zhang C, Gao M, Wang D et al (2017) Relationship between pool characteristic and weld porosity in laser arc hybrid welding of AA6082 aluminum alloy. *J Mater Process Technol* 240:217–222
11. Natio Y, Mizutani M, Katayama S (2003) Observation of keyhole behavior and melt flows during laser-arc hybrid welding. *Proc ICALEO*:41–47
12. Zhang Y, Han S, Cheon J et al (2017) Effect of joint gap on bead formation in laser butt welding of stainless steel. *J Mater Process Technol* 249:274–284
13. Wang J, Nishimura H, Fujii K et al (2009) Study of improvement of gap tolerance in laser MIG arc hybrid welding of aluminium alloy. *Weld Int* 23:723–733
14. Lamas J, Frostevarg J, Kaplan A (2015) Gap bridging for two modes of laser arc hybrid welding. *J Mater Process Technol* 224:73–79
15. Turichin G, Tsibulskiy I, Kuznetsov M et al (2015) Influence of the gap width on the geometry of the welded joint in hybrid laser-arc welding. *Phys Procedia* 78:14–23
16. Pellone L, Inamke G, Hong KM et al (2019) Effects of interface gap and shielding gas on the quality of alloy AA6061 fiber laser lap weldings. *J Mater Process Technol* 268:201–212
17. Brandizzi M, Satriano M, Sorgente D et al (2013) Laser-arc hybrid welding of Ti6Al4V titanium alloy: mechanical characterization of joints and gap tolerance. *Weld Int* 27:113–120
18. Sharma A, Mohanty UK, Tanaka M et al (2021) Mechanism of gap bridge ability in lap-fillet laser-arc hybrid welding. *Lasers Manuf Mater Process* 8:355–371
19. Huang H, Zhang P, Yan H et al (2021) Research on weld formation mechanism of laser-MIG arc hybrid welding with butt gap. *Opt Laser Technol* 133:106530
20. Jing H, Ye X, Hou X et al (2021) The influence of laser power and butt gap on the droplet transfer and weld formation of laser arc hybrid welding. *J Phys: Conf Ser* 2002:012009
21. Wang J, Wang GZ, Wang CM (2015) Mechanisms of the porosity formation during the fiber laser lap welding of aluminium alloy. *Metalurgija* 54:683–686
22. Kawahito Y, Wang H (2018) In-situ observation of gap filling in laser butt weld. *Scr Mater* 154:73–77
23. Zhang K, He C, Liu D et al (2022) Effect of heat input on microstructure and tensile properties of laser welded Ti-3Al-6Mo-2Fe-2Zr alloy joint. *J Mater Res Technol* 17:1652–1661
24. Chen Y, Fan C, Lin S et al (2023) Effect of tungsten inert gas welding parameters on hot crack sensitivity of cast magnesium alloy. *J Mater Eng Perform* 32:1382–1389
25. Liu C, Northwood DO, Bhole SD (2004) Tensile fracture behavior in CO<sub>2</sub> laser beam welds of 7075-T6 aluminum alloy. *Mater Design* 25:573–577
26. Squillace A, Prisco U (2009) Influence of filler material on micro- and macromechanical behaviour of laser-beam-welded T-joint for aerospace applications. *J Mater Des Appl* 223:103–115
27. Kuo T, Lin H (2006) Effects of pulse level of Nd-YAG laser on tensile properties and formability of laser weldments in automotive aluminum alloys. *Mater Sci Eng A* 416:281–289
28. Sepe R, Wiebesiek J, Sonsino CM (2020) Numerical and experimental validation of residual stresses of laser-welded joints and their influence on the fatigue behaviour. *Fatigue Fract Eng Mater Struct* 43:1126–1141

**Publisher's note** Springer Nature remains neutral with regard to jurisdictional claims in published maps and institutional affiliations.

Springer Nature or its licensor (e.g. a society or other partner) holds exclusive rights to this article under a publishing agreement with the author(s) or other rightsholder(s); author self-archiving of the accepted manuscript version of this article is solely governed by the terms of such publishing agreement and applicable law.